

SCIENTIFIC REPORTS



OPEN

Precise Characterisation of Molecular Orientation in a Single Crystal Field-Effect Transistor Using Polarised Raman Spectroscopy

Received: 19 May 2016

Accepted: 17 August 2016

Published: 13 September 2016

Sebastian Wood¹, Grigorios-Panagiotis Rigas^{1,2}, Alina Zoladek-Lemanczyk¹, James C. Blakesley¹, Stamatis Georgakopoulos³, Marta Mas-Torrent³, Maxim Shkunov² & Fernando A. Castro¹

Charge transport in organic semiconductors is strongly dependent on the molecular orientation and packing, such that manipulation of this molecular packing is a proven technique for enhancing the charge mobility in organic transistors. However, quantitative measurements of molecular orientation in micrometre-scale structures are experimentally challenging. Several research groups have suggested polarised Raman spectroscopy as a suitable technique for these measurements and have been able to partially characterise molecular orientations using one or two orientation parameters. Here we demonstrate a new approach that allows quantitative measurements of molecular orientations in terms of three parameters, offering the complete characterisation of a three-dimensional orientation. We apply this new method to organic semiconductor molecules in a single crystal field-effect transistor in order to correlate the measured orientation with charge carrier mobility measurements. This approach offers the opportunity for micrometre resolution (diffraction limited) spatial mapping of molecular orientation using bench-top apparatus, enabling a rational approach towards controlling this orientation to achieve optimum device performance.

Organic semiconductors have attracted interest as a promising alternative to traditional inorganic semiconductors for low cost, light-weight, flexible electronic devices. Their use in various applications has been demonstrated, including light-emitting diodes, photovoltaics, biosensors, and field-effect transistors^{1–4}. The continued development of new organic semiconducting materials, processing techniques, and device architectures demands novel characterisation techniques, in particular, non-destructive, non-invasive measurements that can be deployed in an industrial context.

In this study, we consider specifically the measurement of molecular orientation, which has a profound impact on charge transport within an organic molecular crystal and determines the charge carrier mobility in an electronic device⁵. Multiple studies have shown that tuning the molecular orientation and packing motif using processing conditions, surface interactions, or chemical substitutions can have a profound impact on the resulting charge carrier mobility^{6–11}. Several different techniques have been explored for molecular orientation measurements in thin film organic semiconductors, the most established of which is X-ray diffraction. This has been demonstrated for a number of thin film organic semiconductors, however, a high powered X-ray beam line is usually required to obtain a measurable signal, which limits the spatial resolution for *in situ* studies^{6,9,12,13}. For these reasons, an optical spectroscopic approach is attractive as a more practical technique with micrometre spatial resolution (diffraction limited). Here we demonstrate polarised Raman spectroscopy as a technique for elucidating the orientation of molecules within a single crystal organic field-effect transistor.

The theoretical basis of polarised Raman spectroscopy and its relationship with molecular orientation are well-known, and helpfully reviewed by Tanaka *et al.*^{14,15}. In contrast, the experimental realisation of polarised Raman spectroscopy as a probe of molecular orientation in organic semiconductors has proven challenging^{16–22}.

¹National Physical Laboratory, Hampton Road, Teddington, TW11 0LW, United Kingdom. ²Advanced Technology Institute, University of Surrey, Guildford, GU2 7XH, United Kingdom. ³Institut de Ciència de Materials de Barcelona (ICMAB-CSIC), Campus UAB, 08193 Cerdanyola, Spain. Correspondence and requests for materials should be addressed to S.W. (email: sebastian.wood@npl.co.uk)

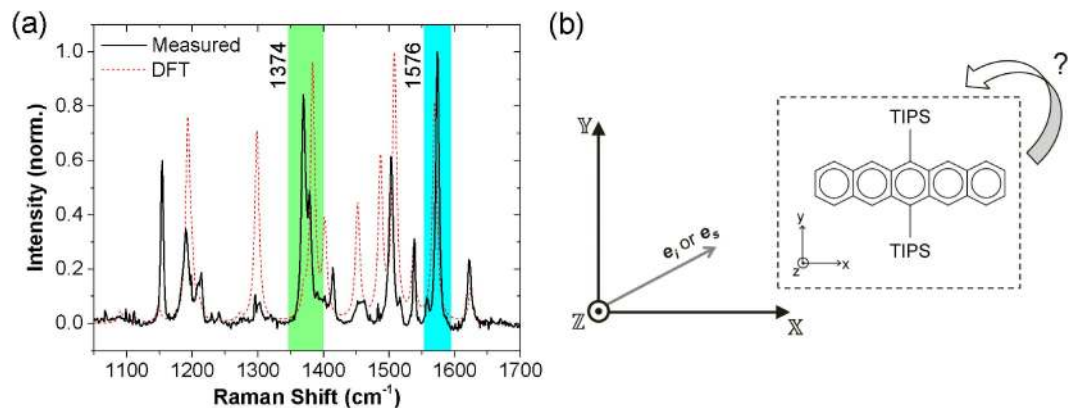


Figure 1. Raman spectrum of TIPS pentacene and illustration of reference frames. (a) Comparison of measured Raman spectrum of TIPS pentacene sample with DFT calculated spectrum showing modes in the range 1050–1700 cm^{-1} measured using 785 nm excitation. Highlighted peaks at 1374 cm^{-1} (green), and 1576 cm^{-1} (blue) are employed to probe the molecular orientation. (b) Diagram showing incident and sampled polarisation vectors (e_i and e_s) within the laboratory frame axes: X , Y and Z . The TIPS pentacene molecule occupies the molecular frame with axes x , y and z , which has an unknown orientation within the laboratory frame.

Published reports have typically focused on pentacene and the soluble derivative 6,13-bis(triisopropylsilyl)ethynyl)pentacene (TIPS pentacene), which readily provide crystalline samples with good charge transport properties. Notably, Mino *et al.* were able to use polarised Raman spectroscopy to characterise the orientation of pentacene molecules in terms of two orientation angles, whereas James *et al.* made a qualitative comparison based on a single orientation angle^{17,18}. However, to fully describe the orientation of a molecule such as pentacene requires three parameters, hence these previous results provide a locus of possible solutions rather than a specific measurement of orientation. Here we address and overcome several experimental limitations in order to demonstrate the characterisation of molecular orientation of TIPS pentacene in a single crystal sample in terms of three Euler coordinates. The measured orientation is in agreement with angle-dependent transistor mobility measurements, and other reports, but suggests a slight difference in interfacial molecular orientation with respect to previous studies based on X-ray diffraction of larger crystals.

Results and Discussion

In the general case, the intensity of polarised Raman scattering from a molecule for a particular vibrational mode, j , is given by:

$$I_s \propto |\mathbf{e}_s \mathbf{R}_j \mathbf{e}_i|^2 \quad (1)$$

where I_s is the intensity of Raman scattering, \mathbf{R}_j is the Raman tensor of mode j for the molecule, \mathbf{e}_i is the electric field vector of the light incident on the molecule (controlled by a polariser), such that the product $\mathbf{R}_j \mathbf{e}_i$ represents the electric field vector of the Raman scattered light, and \mathbf{e}_s is the electric field vector sampled by the instrument (controlled by an analyser). Figure 1(a) shows a typical Raman spectrum of TIPS pentacene, measured with a 785 nm excitation laser. The two strongest Raman peaks are measured at 1374 cm^{-1} and 1576 cm^{-1} , corresponding to collective stretching modes of the acene core of the pentacene molecule, and the relative intensities of these modes show a strong dependence on the molecular orientation arising from the different forms of the Raman tensors for these modes^{14,18}. The pentacene molecule (without TIPS groups) belongs to the D_{2h} point group and the corresponding peaks at 1371 cm^{-1} and 1596 cm^{-1} are assigned to A_g and B_{3g} modes, respectively¹⁷. The Raman tensors for these modes in the molecular frame, with the molecular orientation equivalent to that of the TIPS pentacene in Fig. 1(b), have the general forms:

$$\mathbf{R}'_{A_g} = \begin{pmatrix} a & 0 & 0 \\ 0 & b & 0 \\ 0 & 0 & c \end{pmatrix} \& \mathbf{R}'_{B_{3g}} = \begin{pmatrix} 0 & d & 0 \\ d & 0 & 0 \\ 0 & 0 & 0 \end{pmatrix} \quad (2)$$

where a , b , c , and d are unknown values. Note that the Raman tensor for the B_{3g} mode differs from the usual form for a B_{3g} tensor due to the non-standard molecular orientation used here to facilitate comparison with TIPS pentacene. The addition of TIPS-groups breaks the symmetry of the pentacene molecule such that we expect the Raman tensors to adopt more complex forms. We therefore use density functional theory (DFT) calculations on the TIPS pentacene molecule to optimise the molecular geometry and simulate the Raman scattering (see Experimental Methods for details). The calculated spectrum is compared with the measured case in Fig. 1(a) and the clear correspondence between the measured 1374 cm^{-1} and 1576 cm^{-1} peaks and strong simulated modes enables us to match the measured modes with calculated Raman tensors, whose normalised values are:

$$\mathbf{R}'_{1374} = \begin{pmatrix} -1.00 & -0.0013 & -0.0000027 \\ -0.0013 & -0.34 & -0.00016 \\ -0.0000027 & -0.00016 & -0.037 \end{pmatrix}$$

$$\mathbf{R}'_{1576} = \begin{pmatrix} -0.0014 & 0.79 & 0.00042 \\ 0.79 & 0.0026 & 0.0000016 \\ 0.00042 & 0.0000016 & -0.0000079 \end{pmatrix}. \quad (3)$$

In fact, several elements in these normalised Raman tensors for TIPS pentacene are much less than unity, such that the overall form is similar to the theoretical tensors for pentacene. This is in line with the expectation that the Raman activity of TIPS pentacene is dominated by the conjugated pentacene core, and that the solubilising TIPS groups have little impact on the molecular optoelectronic properties. It is important to recognise that these Raman tensors are valid only in the non-resonant regime and so 785 nm excitation is used for experimental measurements since the sample does not absorb light at this wavelength.

Figure 1(b) shows the molecular structure of TIPS pentacene and its orientation within the molecular frame (x, y, z axes). The Raman tensors (\mathbf{R}') are also calculated in this molecular frame. The laboratory frame ($\mathbb{X}, \mathbb{Y}, \mathbb{Z}$ axes) is defined by the orientation of the instrument and the sample also lies in the laboratory frame. There are multiple ways to describe the orientation of a molecule and no clear consensus in the literature, so we adopt the system of extrinsic Euler coordinates, which is clearly set out by Roy *et al.* where the order of operations is: rotation by ψ about \mathbb{Z} ; followed by rotation by θ around \mathbb{Y} ; followed by rotation by φ around \mathbb{Z} ²³. This gives a direction cosine matrix, \mathbf{D} :

$$\mathbf{D}(\theta, \varphi, \psi) = \begin{pmatrix} \cos \varphi \cos \theta \cos \psi - \sin \varphi \sin \psi & -\cos \varphi \cos \theta \cos \psi - \sin \varphi \cos \theta & \sin \theta \cos \varphi \\ \sin \varphi \cos \theta \cos \psi + \cos \varphi \sin \psi & -\sin \varphi \cos \theta \sin \psi + \cos \varphi \cos \psi & \sin \theta \sin \varphi \\ -\cos \psi \sin \theta & \sin \psi \sin \theta & \cos \theta \end{pmatrix} \quad (4)$$

such that the Raman tensor, \mathbf{R}'_j and spatial coordinates, \mathbf{r}' , defined in the molecular frame can be rotated within the laboratory frame to give \mathbf{R}_j and \mathbf{r} .

$$\mathbf{R}_j = \mathbf{D}\mathbf{R}'_j\mathbf{D}^{-1} \ \& \ \mathbf{r} = \mathbf{D}\mathbf{r}' \quad (5)$$

The objective of the measurement is to elucidate the rotation that must be applied to the molecular frame in order to bring the simulated molecule into the same orientation as the real molecules in the laboratory frame. This is achieved by measuring the polarisation dependence of the Raman scattering intensity. To do this, we vary the polarisation direction of the excitation laser, \mathbf{e}_i using a half-wave plate to rotate the linear polarisation vector through the angle, θ_p . In addition, we use an analyser to sample different polarisation components of the scattered light, where the sampled polarisation, \mathbf{e}_s , is controlled by the orientation angle of the analyser, θ_A . Experimentally, there are multiple components in the optical path with polarisation dependent characteristics (the Rayleigh scattering filter, in particular) resulting in a difference between the linear polarisation direction of the laser beam after the half-wave plate and when it reaches the sample. The polarisation of the scattered light is similarly affected. These effects can be adequately accommodated by introducing the correction factors, k and m , into \mathbf{e}_i and \mathbf{e}_s , which makes the reasonable assumptions that these instrumental factors are symmetric with respect to the \mathbb{X} and \mathbb{Y} axes and have no appreciable impact in the \mathbb{Z} direction²⁴:

$$\mathbf{e}_i = \begin{pmatrix} \cos \theta_p \\ k \cdot \sin \theta_p \\ 0 \end{pmatrix} \ \& \ \mathbf{e}_s = (\cos \theta_A \ m \cdot \sin \theta_A \ 0). \quad (6)$$

In order to obtain values for k and m , we use a silicon wafer reference sample and measure the integrated intensity of the 520 cm^{-1} peak as a function of θ_A and θ_p , the results of which are plotted in Fig. 2(a). The minimum intensity value is subtracted as a first-order correction for partial depolarisation of the incident and scattered light arising in the instrument, and the resulting values are normalised. A more formal accommodation of the partial depolarisation would require an alternative formulation of the system using Mueller calculus, however this would greatly increase the complexity and we find that a good fit between experimental and simulated results can be achieved using our simpler methods.

For the silicon reference sample, the 520 cm^{-1} peak comprises three degenerate modes with the tensors:

$$\mathbf{R}_x = \begin{pmatrix} 0 & 0 & 0 \\ 0 & 0 & f \\ 0 & f & 0 \end{pmatrix} \ \mathbf{R}_y = \begin{pmatrix} 0 & 0 & f \\ 0 & 0 & 0 \\ f & 0 & 0 \end{pmatrix} \ \mathbf{R}_z = \begin{pmatrix} 0 & f & 0 \\ f & 0 & 0 \\ 0 & 0 & 0 \end{pmatrix} \quad (7)$$

in the system with crystal coordinates: $x = [100]$, $y = [010]$, $z = [001]$, and where f is some unknown value²⁵. Substituting these tensors into Equation (1), and using the relationships in Equation (6) we are able to simulate the resulting polarised Raman scattering intensity map corresponding with the experimental measurement. Since the primary flat of the silicon reference sample is parallel to the $\langle 110 \rangle$ direction, a rotation of 45° around the z -axis is required to bring the tensors in Equation (7) into the same orientation as the reference sample. Taking initial values of $k = m = 1$, the least squares difference between the measured and simulated values for a full matrix of θ_A and θ_p values over the measured range is minimised using a MATLAB script to find that the best fit is achieved when $k = 0.829$ and $m = 0.747$. The resulting simulated data are shown in Fig. 2(b).

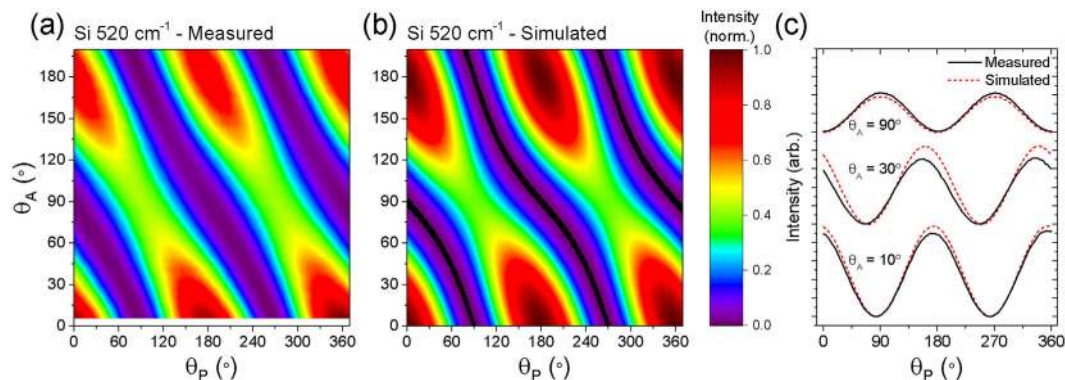


Figure 2. Polarised Raman spectroscopy results for silicon reference sample. Comparison of (a) measured, and (b) simulated plots of the 520 cm^{-1} Raman normalised peak intensity for the silicon reference sample plotted against the polariser angle (θ_p) and analyser angle (θ_A). (c) Compares profiles through the measured and simulated data for $\theta_A = 10, 30, 90^\circ$.

The fitting of the experimental data with the simulated results for the silicon reference sample demonstrates that the model is able to reproduce the main features of the experiment, with the maxima and minima close to the measured θ_A and θ_p values. However, we note that there are some minor discrepancies, particularly in the relative intensities, which are illustrated by the comparison of profiles in Fig. 2(c) for several values of θ_A . Considering silicon to be a good reference material, we attribute the imperfect fitting to the incomplete representation of instrument properties in the model, specifically, the depolarisation effects mentioned above. The impact of these factors on the reliability of the fitting is minimised by collecting data over an extended range of θ_A and θ_p values (in principle, $0 < \theta_A < 90^\circ$ and $0 < \theta_p < 180^\circ$ would give a complete data set).

Using the values for k and m evaluated from the silicon reference sample, we apply the technique to a single crystal of TIPS pentacene, where the molecular orientation is unknown. An image of the sample is given in Fig. 4(a), showing the TIPS pentacene crystal (roughly $150\text{ }\mu\text{m} \times 80\text{ }\mu\text{m}$ laterally with a thickness of 220 nm , estimated using atomic force microscopy) deposited onto a radial array of gold electrodes. These electrodes enable us to make charge transport measurements through the sample using different pairs of electrodes as source and drain to measure transistor mobilities for different orientations of the transistor channel.

In this work we assume an idealised single crystal of TIPS pentacene where all the molecules share a single orientation: in reality we expect some degree of disorder resulting in a distribution of molecular orientations within the sample. In order to obtain sufficient polarised Raman data to assign the measured results to a single molecular orientation, we extract the integrated intensities of both the 1374 cm^{-1} and 1576 cm^{-1} modes. The measurement is also performed with the sample in two different orientations by applying tilt angles to the sample of 0° and 30° around the Y -axis. This is necessary because the results from a single sample orientation will typically yield two indistinguishable solutions, which are reflections of each other in the $\text{X} - \text{Y}$ plane, so by tilting the sample out of this plane these two cases can be distinguished. The intensities of the 1374 cm^{-1} and 1576 cm^{-1} peaks for both tilt angles are shown in Fig. 3(a), with each of the four plots normalised to its own maximum.

As before, a simulation of the polarised Raman scattering measurement is carried out, this time using the calculated Raman tensors given in Equation (3) and substituting the rotated Raman tensors, \mathbf{R}_i , from Equation (5) into Equation (1). Least-squares fitting is used to find the set of Euler coordinates, ψ , θ and φ , which rotate the Raman tensors to give the best fit of the simulation to the experimental data. Figure 3 compares the best fitting simulation results with the measured data. As for the silicon reference sample, the simulation is able to reproduce the main features of the experimental data, but here the imperfect fitting represents a combination of both instrumental factors such as depolarisation, and non-ideal sample properties, such as orientational disorder. The robustness of the result is confirmed by repeating the fitting using a series of 196 combinations of uniformly spaced initial values for the Euler coordinates, and we find that all the best fit values correspond to equivalent molecular orientations (within tolerances of $< 1^\circ$ for each coordinate). The values: $\psi = 68.3^\circ$, $\theta = 118.5^\circ$, $\varphi = -124.6^\circ$ are found to describe the rotation of the TIPS pentacene molecule from the molecular frame into the same orientation as the sample molecules in the laboratory frame. Figure 4(b) represents this molecular orientation by transforming the spatial coordinates of the TIPS pentacene atoms, \mathbf{r}' , (excluding alkyl groups and hydrogen atoms) into the laboratory frame, \mathbf{r} , using equation (5).

Comparing the molecular orientation derived from this method with other published reports reveals a broad agreement. In particular, we note that our solution shows the TIPS groups tilted closest to the substrate, and the shape of the crystal as a whole, shown in Fig. 4(a), is consistent with this orientation too^{26,27}. Importantly, X-ray diffraction (XRD) studies of similar samples typically show the long axis of the pentacene lying near to parallel with the substrate plane, whereas our result shows a small but significant tilt^{13,28,29}. It was not possible to measure XRD data for these single crystal samples due to their size and sensitivity to radiation damage, though this would have enabled a valuable comparison. Rather, this difficulty highlights the need for alternative techniques, such as the one developed here, which can probe molecular orientations non-destructively in small, sensitive samples. XRD studies on larger samples have shown that the molecular packing of various acene derivatives depends on

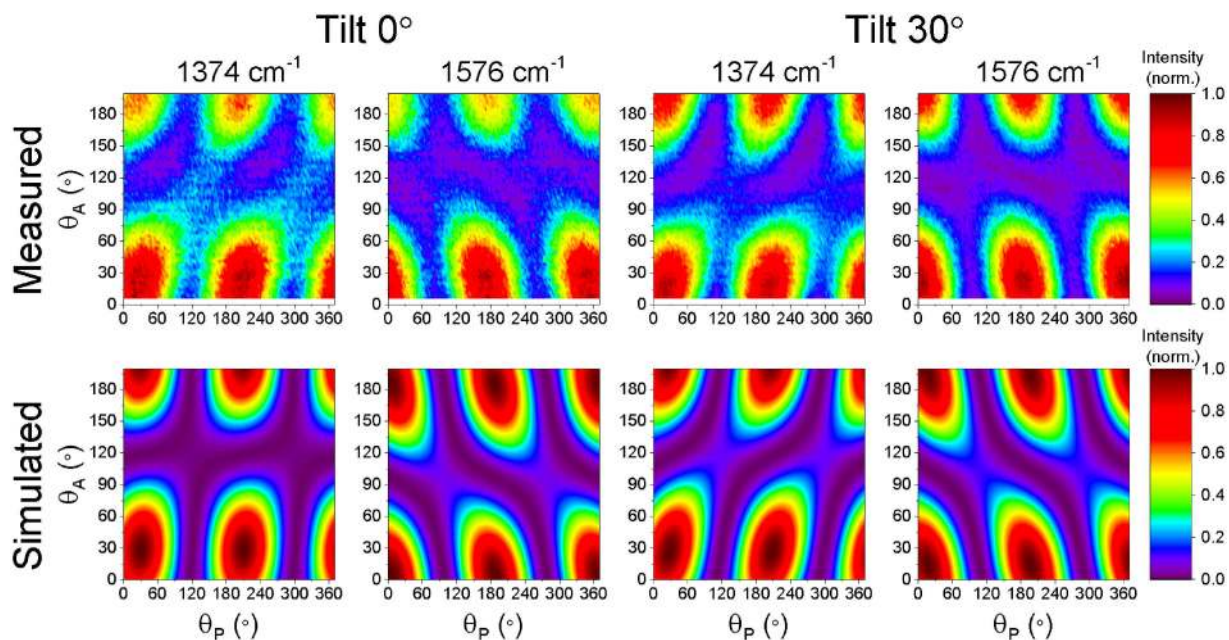


Figure 3. Polarised Raman spectroscopy results for TIPS pentacene sample. Comparison of measured (top) polarised Raman data with the best fitting simulated results (bottom). The intensities of the 1374 cm^{-1} and 1576 cm^{-1} modes measured with tilts of both 0° and 30° around the \bar{Y} -axis are considered. In each plot the normalised intensity of the Raman peak is plotted against the polariser angle (θ_P) and analyser angle (θ_A).

crystallite size and growth conditions, and so it is reasonable to conclude that the result presented here reveals a real phenomenon^{6,22,30}.

The charge transport in TIPS pentacene crystals is anisotropic since the charge transfer is mediated through overlapping π -orbitals of the acene core and the molecules adopt a ‘brick-wall’ packing motif^{10,31}. We can therefore verify the molecular orientation, measured using polarised Raman spectroscopy, by comparing this with the angular dependent charge mobility using the transistor structure shown in Fig. 4(a). Three different transistor channels are formed in the sample with angles of 0° , 30° and 60° between the charge transport direction and the \bar{X} -axis. We expect to measure the lowest charge mobility when the acene core is aligned parallel with the channel length and higher values when it is aligned at a more oblique angle. The limited number of devices available in this sample mean that quantitative conclusions cannot be drawn, but the transfer characteristics and mobility values shown in Fig. 4(c) show a significantly higher mobility for the device with a 0° channel angle, corresponding with an angle of $\sim 40^\circ$ between the channel orientation and the $\bar{X} - \bar{Y}$ projection of the acene core, than for the 30° and 60° devices, where the acene is closer to parallel to the channel current.

Conclusions

This study has demonstrated the use of polarised Raman spectroscopy as a probe for molecular orientation, taking the example of a TIPS pentacene single crystal transistor as a model system. Importantly, we have been able to express the solution quantitatively using Euler coordinates to fully describe the orientation of the molecule with respect to the substrate. This work opens the way for meaningful and unambiguous measurements of molecular orientation using a non-destructive, non-invasive, bench-top technique capable of offering diffraction-limited lateral resolution. Further refinement of this method might be achieved by incorporating additional factors into the simulation to account for instrumental depolarisation effects more explicitly, or with additional parameters to describe the orientational disorder present in the sample. In the example considered here, the molecular orientation of TIPS pentacene in the small single crystal is found to differ slightly from that reported for larger crystals. Subtle modifications to the bulk molecular packing motif in thin films have been found to have dramatic impacts on the charge transport properties of organic semiconductors, and so polarised Raman spectroscopy offers a particularly appropriate tool for probing molecular orientations in thin film or microstructured devices. Combining this technique with methods to control the molecular orientation provides a way to intelligently tune the fabrication conditions for optimised performance of organic molecular electronics.

Experimental Methods

Sample Preparation. A circular array of Au electrodes was patterned on top of a SiO_2/Si substrate using conventional photolithography³². The substrate used was n++ Si with 200 nm thermally grown SiO_2 (purchased from Si-Mat). S1813 positive photoresist was spin-coated at 4000 rpm, followed by baking at 100°C for 1 min. The photoresist was patterned with a laser writer (Durham magneto-optics) at 405 nm with a dose of $150\text{ mJ}/\text{cm}^2$. The sample was developed with MF319 developer for 1 min and rinsed with deionised H_2O . Subsequently the metal layers were evaporated; 5 nm of Cr (rate $0.3\text{ \AA}/\text{s}$) followed by 35 nm of Au (rate $0.5\text{ \AA}/\text{s}$). Lift-off was performed by

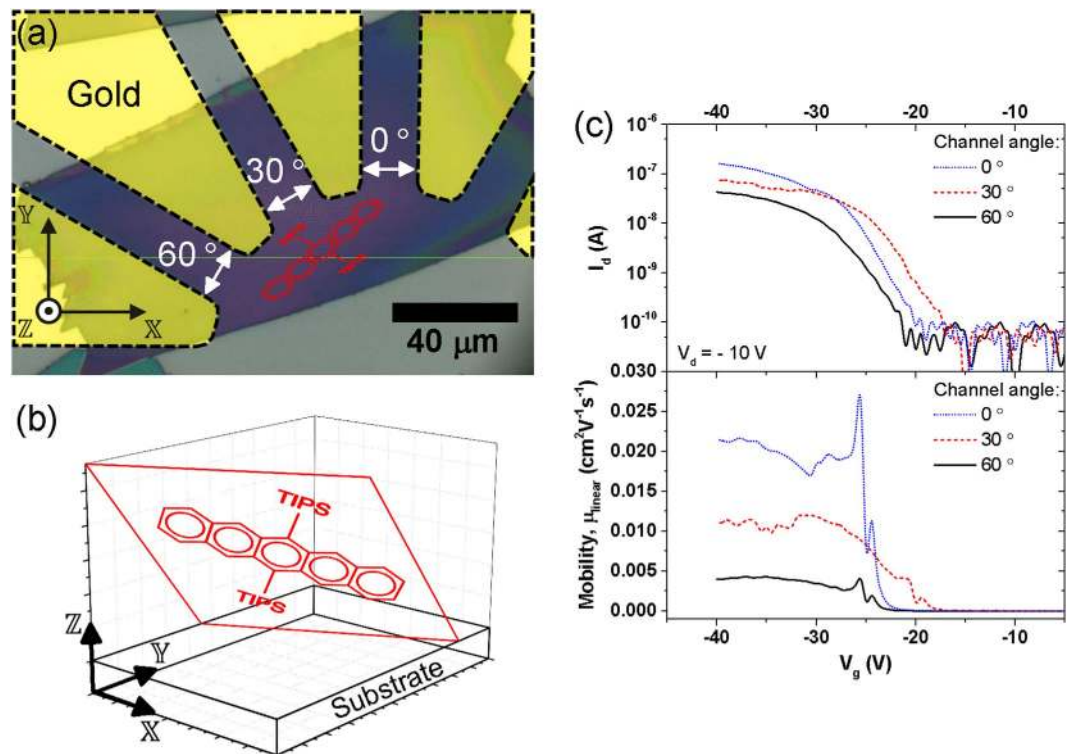


Figure 4. Orientation dependence of charge carrier mobility in TIPS pentacene sample. (a) Microscope image of sample showing a TIPS pentacene crystal deposited on top of an array of radial gold electrodes (outlined and highlighted) to form transistor channels with different angles (0° , 30° , and 60°) between the charge transport direction (white arrows) and X -axis. The orientation of the TIPS pentacene molecule is shown in red, projected on to the $X - Y$ plane. (b) Plot showing the TIPS pentacene molecular structure in its measured orientation with respect to the substrate in the laboratory frame (plane of the acene backbone also shown for clarity). (c) Comparison of measured transfer characteristics (top) and estimated hole mobilities assuming the linear operation regime (bottom) for transistor channels at 0° , 30° , and 60° .

sonicating in acetone and further cleaning by sonicating in HPLC grade acetone and isopropanol. For the single crystals, 2 mg of TIPS-pentacene, synthesised with previously described techniques²⁸, was dissolved in 1 mL of toluene. The solution was spray-printed, using a previously reported technique³³, on top of the electrodes forming single crystals. The electrode/organic and dielectric/organic interfaces were not modified using any self-assembled monolayer prior to the crystal deposition.

The lateral dimensions of the crystal were measured using optical microscopy, and the vertical thickness measured by atomic force microscopy using an MFP-3D (Asylum Research) instrument in tapping mode. Line profiles across the crystal edge were measured in three places giving values of 221, 220, and 210 nm as approximations for the crystal thickness.

Polarised Raman Spectroscopy. Raman spectra were measured using a Horiba HR800 Evolution Labram Spectrometer. A 785 nm excitation laser was used with a half-wave plate polariser and an analyser for polarised measurements. The angular position of the polariser, P , is related to θ_p and the resulting orientation of the incident polarisation vector, e_p , using: $\theta_p = 364.6^\circ - 2P$, which accounts for the behaviour of the half-wave plate and also an offset from zero of the polariser position. Similarly, the position of the analyser, A , relates to θ_A and the orientation of the sampled polarisation vector, e_s , using: $\theta_A = 5.7^\circ + A$. The sample is mounted on a ThorLabs PRM1/MZ8 rotating stage to control the sample tilt around the Y -axis. Polarisation dependent Raman plots were acquired for all points in the range $0 < P < 190$ in 1.5° steps, and $0 < A < 200$ in 3° steps with a 1 s acquisition time at each point. The laser power at the sample was ~ 10 mW for TIPS pentacene samples and ~ 100 mW for the silicon reference. No change in the Raman spectrum of pentacene was observed after multiple excitations indicating that no significant sample degradation occurred during the measurement. A $50\times$ long working distance objective was used throughout to accommodate the tilting of the sample up to 30° out of plane, the numerical aperture of this objective (0.45) is sufficiently low enough that the depolarisation effect introduced by focusing the laser beam is not expected to be problematic¹⁴.

DFT Calculations. DFT calculations were carried out using the GAUSSIAN09 software package to optimise the geometry of the TIPS pentacene molecule and then perform frequency analysis^{34,35}. The B3LYP hybrid

functional and the 6–31G(d,p) basis set were used^{36–39}. The alkyl groups were truncated to minimise the computational requirements, and Raman tensors were extracted using a script developed by the Schlegel group⁴⁰.

Device Characterisation. For the electrical characterisation, a Keithley 4200 semiconductor characterisation system was used. Each transistor channel was defined by the fixed distance between the electrodes ($L = 20 \mu\text{m}$) and the width, W , of the crystal that was crossing it ($W(60^\circ \text{ device}) = 70 \mu\text{m}$, $W(30^\circ \text{ device}) = 40 \mu\text{m}$, $W(0^\circ \text{ device}) = 60 \mu\text{m}$) - see Fig. 4(a). The field effect mobility of each device was extracted using the standard MOSFET equation in the linear regime: $\mu^{\text{linear}} = \frac{L}{WC_0 V_{sd}} \frac{\partial I_{sd}}{\partial V_{gs}}$.

References

- Jou, J.-H., Kumar, S., Agrawal, A., Li, T.-H. & Sahoo, S. Approaches for fabricating high efficiency organic light emitting diodes. *J. Mater. Chem. C* **3**, 2974–3002 (2015).
- Dou, L. *et al.* 25th Anniversary Article: A Decade of Organic/Polymeric Photovoltaic Research. *Adv. Mater.* **25**, 6642–6671 (2013).
- Lin, P. & Yan, F. Organic Thin-Film Transistors for Chemical and Biological Sensing. *Adv. Mater.* **24**, 34–51 (2012).
- Sirringhaus, H. 25th Anniversary Article: Organic Field-Effect Transistors: The Path Beyond Amorphous Silicon. *Adv. Mater.* **26**, 1319–1335 (2014).
- Mas-Torrent, M. & Rovira, C. Role of molecular order and solid-state structure in organic field-effect transistors. *Chem. Rev.* **111**, 4833–4856 (2011).
- Giri, G. *et al.* Tuning charge transport in solution-sheared organic semiconductors using lattice strain. *Nature* **480**, 504–508 (2011).
- Dou, J.-H. *et al.* Fine Tuning of Crystal Packing and Charge Transport Properties of BDOPV Derivatives through Fluorine Substitution. *J. Am. Chem. Soc.* **137**, 15947–15956 (2015).
- Tumbleston, J. R. *et al.* The influence of molecular orientation on organic bulk heterojunction solar cells. *Nat. Photonics* **8**, 385–391 (2014).
- Sirringhaus, H. *et al.* Two-dimensional charge transport in conjugated polymers. *Nature* **401**, 685–688 (1999).
- Wade, J. *et al.* Charge mobility anisotropy of functionalized Pentacenes in organic field effect transistors fabricated by solution processing. *J. Mater. Chem. C* **2**, 10110–10115 (2014).
- Sun, X., Di, C. & Liu, Y. Engineering of the dielectric–semiconductor interface in organic field-effect transistors. *J. Mater. Chem.* **20**, 2599 (2010).
- DeLongchamp, D. M., Kline, R. J. & Herzog, A. Nanoscale structure measurements for polymer–fullerene photovoltaics. *Energy Environ. Sci.* **5**, 5980–5993 (2012).
- Mannsfeld, S. C. B., Tang, M. L. & Bao, Z. Thin film structure of triisopropylsilylethynyl-functionalized pentacene and tetraceno[2,3-b]thiophene from grazing incidence x-ray diffraction. *Adv. Mater.* **23**, 127–131 (2011).
- Tanaka, M. & Young, R. J. Review Polarised Raman spectroscopy for the study of molecular orientation distributions in polymers. *J. Mater. Sci.* **41**, 963–991 (2006).
- Adar, F. & Noether, H. Raman microprobe spectra of spin-oriented and drawn filaments of poly(ethylene terephthalate). *Polymer* **26**, 1935–1943 (1985).
- Seto, K. & Furukawa, Y. Study on solid structure of pentacene thin films using Raman imaging. *J. Raman Spectrosc.* **43**, 2015–2019 (2012).
- Mino, T., Saito, Y., Yoshida, H., Kawata, S. & Verma, P. Molecular orientation analysis of organic thin films by z-polarization Raman microscope. *J. Raman Spectrosc.* **43**, 2029–2034 (2012).
- James, D. T. *et al.* Thin-film morphology of inkjet-printed single-droplet organic transistors using polarized Raman spectroscopy: effect of blending TIPS-pentacene with insulating polymer. *ACS Nano* **5**, 9824–9835 (2011).
- Hosoi, Y., Deyra, D. M., Nakajima, K. & Furukawa, Y. Micro-Raman Spectroscopy on Pentacene Thin-Film Transistors. *Mol. Cryst. Liq. Cryst.* **491**, 317–323 (2008).
- Onojima, N., Nakamura, A., Saito, H. & Daicho, N. Aligned growth of TIPS pentacene crystalline domains adhered to Au stripes formed on SiO₂ surfaces. *J. Cryst. Growth* **432**, 146–151 (2015).
- Cheng, H. L., Chou, W. Y., Kuo, C. W., Tang, F. C. & Wang, Y. W. Electric field-induced structural changes in pentacene-based organic thin-film transistors studied by *in situ* micro-Raman spectroscopy. *Appl. Phys. Lett.* **88**, 1–3 (2006).
- Xu, J. *et al.* Probing the interfacial molecular packing in TIPS-pentacene organic semiconductors by surface enhanced Raman scattering. *J. Mater. Chem. C* **2**, 2985–2991 (2014).
- Roy, S., Hung, K.-K., Stege, U. & Hore, D. K. Rotations, Projections, Direction Cosines, and Vibrational Spectra. *Appl. Spectrosc. Rev.* **49**, 233–248 (2013).
- Becker, M., Scheel, H., Christiansen, S. & Strunk, H. P. Grain orientation, texture, and internal stress optically evaluated by micro-Raman spectroscopy. *J. Appl. Phys.* **101**, 063531 (2007).
- Wolf, I. De. Micro-Raman spectroscopy to study local mechanical stress in silicon integrated circuits. *Semicond. Sci. Technol.* **11**, 139–154 (1996).
- Chen, J. *et al.* Thermal and Mechanical Cracking in Bis(triisopropylsilylethynyl) Pentacene Thin Films. *J. Polym. Sci. Part B Polym. Phys.* **44**, 3631–3641 (2006).
- James, D. T., Frost, J. M., Wade, J., Nelson, J. & Kim, J. Controlling Microstructure of Pentacene Derivatives by Solution Processing: Impact of Structural Anisotropy on Optoelectronic Properties. *ACS Nano* **7**, 7983–7991 (2013).
- Anthony, J. E., Brooks, J. S., Eaton, D. L. & Parkin, S. R. Functionalized Pentacene: Improved Electronic Properties from Control of Solid-State Order. *J. Am. Chem. Soc.* **123**, 9482–9483 (2001).
- Chen, J., Martin, D. C. & Anthony, J. Morphology and molecular orientation of thin-film bis(tri-isopropylsilylethynyl) pentacene. *J. Mater. Res.* **22**, 1701–1709 (2007).
- Gnoli, A. *et al.* Bis(triisopropylsilylethynyl)pentacene/Au(111) Interface: Coupling, Molecular Orientation, and Thermal Stability. *J. Phys. Chem. C* **118**, 22522–22532 (2014).
- Ostroverkhova, O. *et al.* Anisotropy of transient photoconductivity in functionalized pentacene single crystals. *Appl. Phys. Lett.* **89**, 192113 (2006).
- Reese, C. & Bao, Z. High-resolution measurement of the anisotropy of charge transport in single crystals. *Adv. Mater.* **19**, 4535–4538 (2007).
- Rigas, G.-P., Payne, M. M., Anthony, J. E., Castro, F. A. & Shkunov, M. Spray-printing of isolated semiconducting organic single crystals. (*Submitted*) (2016).
- Imperial College High Performance Computing Service. <http://www.imperial.ac.uk/ict/services/teachingandresearchservices/highperformancecomputing>.
- Frisch, M. J. *et al.* Gaussian 09, Revision A.1 (2009).
- Becke, A. D. Density-functional thermochemistry. III. The role of exact exchange. *J. Chem. Phys.* **98**, 5648–5652 (1993).
- Lee, C., Yang, W. & Parr, R. G. Development of the Colle-Salvetti correlation-energy formula into a functional of the electron density. *Phys. Rev. B* **37**, 785–789 (1988).

38. Petersson, G. A. *et al.* A complete basis set model chemistry. I. The total energies of closed-shell atoms and hydrides of the first-row elements. *J. Chem. Phys.* **89**, 2193–2218 (1988).
39. Petersson, G. A. & Al-Laham, M. A. A complete basis set model chemistry. energies of the first-row atoms II. Open-shell systems and the total. *J. Chem. Phys.* **94**, 6081–6090 (1991).
40. Gaussian Archive Reader. Available at: <http://chem.wayne.edu/schlegel/Software.html>.

Acknowledgements

This work was funded by the Department for Business, Innovation & Skills through the National Measurement System as part of the Innovation, Research and Development programme. M.S. acknowledges equipment funding from EPSRC UK Grant EP/I017569/1. S.G. and M.T would like to acknowledge the financial support from ERC StG 2012-306826 e-GAMES project and CIBER-BBN. Thanks are due to Prof. J.E. Anthony and his group from the University of Kentucky, for synthesising the functionalised pentacene derivative used in this work, and also, to J. Wade at Imperial College London for the DFT calculations.

Author Contributions

S.W. and A.Z.-L. performed spectroscopic measurements. G.-P.R. and S.G. designed and fabricated the transistor sample. G.-P.R. performed electrical characterisation. S.W., J.C.B. and F.A.C. developed the computational model. S.W., J.C.B. and F.A.C. wrote the manuscript. F.A.C., M.S. and M.M.-T. contributed materials and analysis tools. All authors reviewed the manuscript.

Additional Information

Competing financial interests: The authors declare no competing financial interests.

How to cite this article: Wood, S. *et al.* Precise Characterisation of Molecular Orientation in a Single Crystal Field-Effect Transistor Using Polarised Raman Spectroscopy. *Sci. Rep.* **6**, 33057; doi: 10.1038/srep33057 (2016).



This work is licensed under a Creative Commons Attribution 4.0 International License. The images or other third party material in this article are included in the article's Creative Commons license, unless indicated otherwise in the credit line; if the material is not included under the Creative Commons license, users will need to obtain permission from the license holder to reproduce the material. To view a copy of this license, visit <http://creativecommons.org/licenses/by/4.0/>

© The Author(s) 2016